Cell. Mol. Life Sci. (2011) 68:1269–1281
DOI 10.1007/s00018-010-0524-2

Cellular and Molecular Life Sciences

RESEARCH ARTICLE

Plant ribosome-inactivating proteins type II induce the unfolded protein response in human cancer cells

C. Horrix · Z. Raviv · E. Flescher · C. Voss · M. R. Berger

Received: 3 July 2010 / Revised: 9 August 2010 / Accepted: 30 August 2010 / Published online: 16 September 2010

Abstract Cytotoxic ribosome-inactivating proteins (RIPs) of type II such as ricin were investigated as anti-cancer agents, but also pose a threat as biological weapons. The molecular mechanism leading to their toxic effects is, however, not yet clear. The current paradigm, which states that the irreversible depurination of 28S rRNA results in a general translational arrest eventually leading to cell death, has been questioned. Using micro-array, qRT-PCR and Western blot, we identified the unfolded protein response (UPR), a cellular mechanism activated in response to endoplasmic reticulum stress, that is induced in HCT116 and MDA-MB-231 cells exposed to the plant type II RIPs ricin, riproximin and volkensin. Apoptosis was induced by concentrations at which translation of UPR-related genes still occurred, despite concomitant ribosomal depurination. We conclude that UPR induction represents a model that better describes the cellular effects of RIP exposure at concentrations at which selected proteins are translated despite ribosomal depurination.

Keywords Ricin · Riproximin · Volkensin · Anti-cancer · Bio-weapon · Depurination · RIP · UPR

Abbreviations

RIP	Ribosome-inactivating protein
ERS	Endoplasmic reticulum stress
UPR	Unfolded protein response
PERK	(Protein kinase RNA-activated)-like endoplasmic reticulum kinase
IRE1	Inositol-requiring protein 1
ATF6	Activating transcription factor 6
eIF2α	Eukaryotic translation initiation factor 2 subunit α
ATF	Activating transcription factor
GADD	Growth arrest and DNA damage inducible gene
ID1	Inhibitor of differentiation 1
XBP-1	X-box binding protein 1
EDEM1	ER degradation enhancer, mannosidase alpha-like 1
RAMP4	Ribosome-attached membrane protein 4
HEDJ	Human ER-associated dnaJ protein
GLS	Golgi localization sequence

Electronic supplementary material The online version of this article (doi:10.1007/s00018-010-0524-2) contains supplementary material, which is available to authorized users.

C. Horrix · M. R. Berger (✉)
Toxicology and Chemotherapy Unit,
German Cancer Research Center,
Im Neuenheimer Feld 581, 69120 Heidelberg, Germany
e-mail: M.Berger@dkfz-heidelberg.de

C. Horrix
e-mail: c.horrix@dkfz.de

Z. Raviv · E. Flescher
Department of Clinical Microbiology and Immunology,
Sackler School of Medicine, Tel-Aviv University,
Ramat Aviv, 69978 Tel Aviv, Israel

Z. Raviv
e-mail: zraviv06@gmail.com

E. Flescher
e-mail: flascher@post.tau.ac.il

C. Voss
Department of Biochemistry, Heidelberg Pharma AG,
Schriesheimer Strasse 101, 68526 Ladenburg, Germany
e-mail: C.Voss@hdpharma.com

Introduction

Ricin is a highly toxic lectin from the plant *Ricinus communis*, which has been investigated for its anti-neoplastic potential. Due to the good availability of *R. communis*, ricin's easy purification and high cytotoxicity, it has been listed as a level B biothreat by the US Centers for Disease Control and Prevention (CDC) [1]. Ricin belongs to the class of type II ribosome-inactivating proteins (RIPs). In contrast to type I RIPs consisting of a single A-chain, proteins of the type II RIP group consist of two polypeptide chains, designated as A- and B-chains, which are connected by a disulfide bridge. The B-chain is a lectin with affinity for certain sugar moieties, with each type II RIP showing distinct sugar specificity. The A-chain of all RIPs is an rRNA *N*-glycosylase (EC 3.2.2.22) able to hydrolyze a specific adenine from the ricin/sarcin loop of the ribosomal 28S RNA. This depurination eventually leads to an irreversible damage of the ribosomes and to protein translation inhibition, finally resulting in cell death [2].

Many toxic type II RIPs, including prominent examples like ricin and viscumin [3], were shown to be more toxic to cancer than to normal cells and have therefore been repeatedly assessed as anti-cancer agents. However, an unexpectedly high unspecific toxicity of ricin has precluded its development as an anti-cancer drug. To override these problems, which were shown to be caused by unspecific binding of the B-chain to several tissues, conjugates of the enzymatically active A-chain linked to various carriers, especially antibodies, were developed [3]. As a most recent example, the ricin A-chain derived immunoconjugate Combotox was reported to have significant effects in children with refractory leukaemia [4].

The mode of action of RIPs was postulated to depend on the translational arrest caused by irreversible ribosome damage. This mechanism was confirmed for several newly discovered plant type II RIPs, including riproximin. Riproximin, a new type II RIP, was isolated as the active component of a powdered plant material, anecdotally described to possess anti-neoplastic activity. Ingestion of this plant powder, commonly used in African traditional medicine, was described to be associated with remission of metastatic prostate cancer in patients. Riproximin showed high anti-proliferative activity in a panel of cancer cell lines, as well as distinct anti-neoplastic activity in a rat colorectal cancer liver metastasis model. The concentrations causing growth arrest in non-transformed cell lines were 10- to 100-fold higher than concentrations that were cytotoxic in several highly sensitive cancer cell lines. The mechanism of action typical for RIPs was confirmed for riproximin in a cell-free system. However, the protein synthesis inhibiting concentrations were at least two orders of magnitude higher than those required to cause growth arrest [5, 6]. Moreover, it was observed that cells exposed to riproximin were still able to perform some protein synthesis [7]. Therefore, the question arose whether the ribosome inactivation and subsequent translational arrest were indeed the only factors responsible for the induction of cell death. A limited gene expression micro-array study indicated that an endoplasmic reticulum stress (ERS) response may play a role in the cellular reaction to riproximin [7].

An ERS response is triggered when the homeostasis of the ER is disturbed by accumulation of unfolded proteins in the ER lumen. That causes the induction of three signaling cascades—summarized under the term unfolded protein response (UPR)—which converge to elicit three effects: the general protein translation is decreased, special UPR-related proteins like chaperones and foldases are induced, and the ER-associated degradation (ERAD) machinery is activated. When all these mechanisms fail to reduce the load of unfolded proteins in the ER, the cell dies of apoptosis or autophagy [8–10]. The three signaling cascades are triggered by activation of the three transducers PERK [(protein kinase RNA-activated)-like endoplasmic reticulum kinase], IRE1 (inositol-requiring protein 1) and activating transcription factor 6 (ATF6), which are localized in the ER membrane [11] (Fig. 1). They are activated as soon as the chaperone BiP (immunoglobulin heavy chain-binding protein), which normally masks the luminal domains of these sensors, is titrated away by unfolded proteins. Hereupon PERK and IRE1 are activated by *trans*-autophosphorylation and transmit the signal into the cytosol by different cascades. Activated PERK phosphorylates and thereby inhibits eIF2α (eukaryotic translation initiation factor two subunit α), which is a necessary factor for the initiation of translation. This results in two apparently opposite effects, i.e., a general translational arrest and enhanced translation of specially structured mRNAs like activating transcription factor 4 (ATF4). Translated ATF4 induces the transcription of ATF3 (activating transcription factor 3) and GADD153 (growth arrest and DNA damage inducible gene 153) in the nucleus, which are transcription factors themselves [12, 13]. For instance, ATF3 is known to negatively regulate the expression of inhibitor of differentiation 1 (ID1), which exerts anti-apoptotic effects [14].

The third transducer ATF6 has another mode of activation. After detachment of BiP, its Golgi localization sequence (GLS) mediates the transport of the 90-kDa protein ATF6 to the Golgi apparatus, where it is sequentially cleaved by S1 (site 1) and S2 (site 2) proteases. The result is a 50-kDa N-terminal transcription factor that is able to activate certain UPR and ERAD genes, including X-box binding protein 1 (XBP-1) in the nucleus. The mRNA of XBP-1 is alternatively spliced by activated IRE1 [15],

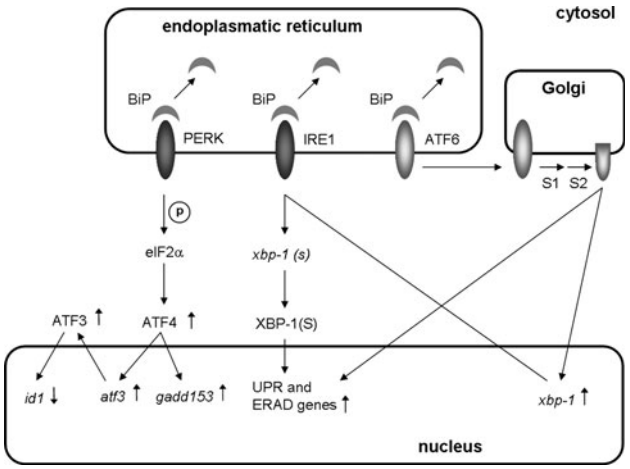

Fig. 1 Simplified schematic illustration of the unfolded protein response. The UPR cascade and the localization of its components within the cellular compartments are given at mRNA (*small italic letters*) and protein (*capital letters*) levels

leading to a frameshift and thereby abolishing a stop codon. After translation, this results in an increased protein level of a 54-kDa spliced active transcription factor [XBP-1(S)] instead of a 28-kDa unspliced protein [XBP-1(U)]. XBP-1(S) translocates into the nucleus and activates ERAD components as well as several chaperones and foldases, which play a role in protein folding, maturation, secretion and degradation [16].

Since toxic type II RIPs are known to accumulate in the ER upon cell entry [17], it is conceivable that ER stress might occur in cells exposed to the toxic members of this class of agents. To answer this question, the two prominent, highly toxic type II RIPs ricin and volkensin were included in this study, in addition to riproximin.

Materials and methods

Cell culture

The human adenocarcinoma cell lines MDA-MB-231 (breast) and HCT116 (colon) were obtained from ATCC (no. HTB-26 and CCL-247) and cultured in RPMI-1640 and McCoy's 5A medium, respectively. All media were supplemented with 10% FCS and 2 mM L-glutamine. The cells were propagated at 37°C in a humidified atmosphere with 5% CO_2.

Reagents and antibodies

Riproximin was isolated and purified from kernels of *Ximenia americana* according to Voss et al. [5] with some modifications (unpublished details). Ricin and volkensin were a kind gift of Dr. Fiorenzo Stirpe (University of Bologna, Italy). MTT was obtained from SERVA Electrophoresis (Heidelberg, Germany), culture media and L-glutamine from Invitrogen (Darmstadt, Germany) and FCS from PAA Laboratories (Pasching, Austria). Protease-inhibitor-cocktail Complete Mini, EDTA-free was purchased from Roche Applied Science (Penzberg, Germany), Mowiol from Carl Roth (Karlsruhe, Germany) and DAPI (4′,6-diamidin-2-phenylindol) from Sigma-Aldrich (Steinheim, Germany). The primary antibodies against ATF3 (sc-188), ATF6α (sc-22799), ERK2 (sc-1647) and XBP-1 (sc-32135) were purchased from Santa Cruz Biotechnology (Heidelberg, Germany); those against CHOP/GADD153 (2895), PARP (9541), eIF2α (9722), phospho-eIF2α (9721) and Caspase-7 (9491) were ordered from Cell Signaling Technology (Danvers, MA). The secondary antibodies anti-goat (sc-2020), anti-rabbit (sc-2054) and anti-mouse (sc-2055) were obtained from Santa Cruz Biotechnology.

Viability assay

A total of 3×10^3 cells per well were plated in 96-well tissue culture plates (BD Bioscience, Franklin Lakes, NJ). After overnight incubation at 37°C and 5% CO_2, the cells were exposed to various concentrations of ricin, riproximin or volkensin for another 24 h. Cell viability was determined using the MTT assay as previously reported [5]. Data are given as mean ± SE of three to seven independent experiments, each performed in triplicate.

Isolation of total RNA and protein

A total of 2.5×10^6 cells were seeded in tissue culture plates (146 mm diameter; TPP, Trasadingen, Switzerland) and cultured for 24 h. The following day the cells were exposed to the concentrations of ricin, riproximin or volkensin for 24 h as indicated in Figs. 2, 3, 4, 5, 6. Then the cells were harvested and RNA was isolated with the RNeasy Mini Kit (Qiagen, Hilden, Germany) according to the manufacturer's instructions. Residual genomic DNA was digested using the Turbo DNA-free kit (Applied Biosystems, Darmstadt, Germany). For isolation of total protein, cells were lysed with 1 ml/10^7 cells of modified RIPA buffer [50 mM Tris-HCl (pH 7.4); 1% NP-40; 0.25% Na-deoxycholat; 150 mM NaCl; 1 mM EDTA; 1 mM NaF, protease-inhibitor-cocktail Complete Mini, EDTA-free] at 4°C for 15 min with occasional shaking. The lysates were centrifuged for 15 min at 4°C and 14,000×*g*; the resulting supernatants were immediately transferred to fresh tubes. The protein concentration was determined using the CB-X Protein Assay (G-Biosciences, Maryland Heights, MO).

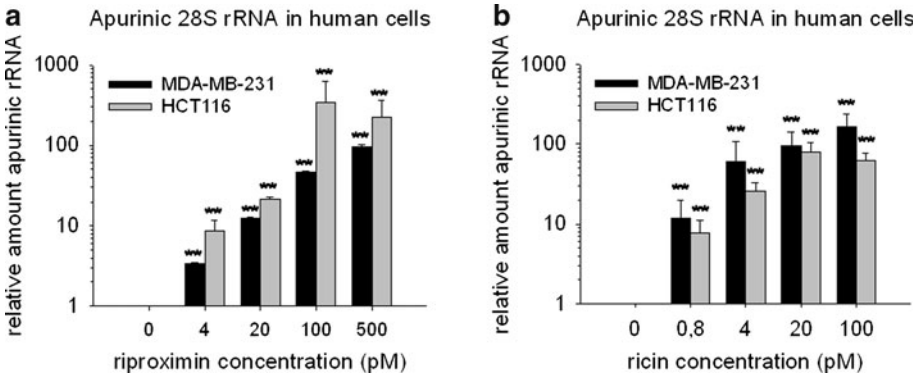

Fig. 2 Depurination of the 28S rRNA by riproximin and ricin. MDA-MB-231 and HCT116 cells were incubated for 24 h with a range of riproximin **a** or ricin **b** concentrations as indicated in the respective charts. The resulting relative amount of apurinic sites in 28S rRNA compared to untreated controls was determined by qRT-PCR. 28S rRNA aside from the depurination site was used for normalization of the samples. Data are given as mean fold change ± standard error (*SE*) of two independent experiments, each performed in triplicate. $^{**}p < 0.005$ (comparison between control and treatment)

Micro-array probe labeling and Illumina Sentrix BeadChip array hybridization

The quality of total RNA was checked by gel analysis using the total RNA Nano chip assay on an Agilent 2100 Bioanalyzer (Agilent Technologies, Berlin, Germany). The RNA index values of the samples ranged between 8.8 and 10.

Biotin-labeled cRNA samples for hybridization on Illumina Human Sentrix-8 BeadChip arrays (Illumina, San Diego, CA) were prepared according to Illumina's recommended sample labeling procedure based on the modified Eberwine protocol [18]. In brief, 250 ng total RNA was used for cDNA synthesis, followed by an amplification/labeling step (in vitro transcription) to synthesize biotin-labeled cRNA according to the MessageAmp II aRNA Amplification kit (Ambion, Austin, TX). Biotin-16-UTP was purchased from Roche Applied Science. The cRNA was column purified according to TotalPrep RNA Amplification Kit and eluted in 60 µl of water. Quality of cRNA was controlled using the RNA Nano Chip Assay on an Agilent 2100 Bioanalyzer and spectrophotometrically quantified. Hybridization was performed at 58°C in GEX-HCB buffer (Illumina) at a concentration of 100 ng cRNA/µl, unsealed in a wet chamber for 20 h. Spike-in controls for low, medium and highly abundant RNAs were added, as well as mismatch control and biotinylation control oligonucleotides. Micro-arrays were washed twice in E1BC buffer (Illumina) at room temperature for 5 min. After blocking for 5 min in 4 ml of 1% (w/v) blocker casein in phosphate-buffered saline of Hammarsten grade (Pierce Biotechnology, Rockford, IL, USA), array signals were developed by a 10-min incubation in 2 ml of 1 µg/ml Cy3-streptavidin (Amersham Biosciences, Buckinghamshire, UK) solution and 1% blocking solution. After a final wash in E1BC, the arrays were dried and scanned.

Micro-array scanning and data analysis

Micro-array scanning was performed on a Beadstation array scanner, with the setting adjusted to a scaling factor of 1 and PMT settings at 430. Data extraction was performed for all beads individually, and outliers were removed when >2.5 median absolute deviation (MAD). All remaining data points were used for the calculation of the mean average signal for a given probe, and SD for each probe was calculated. Data analysis was performed by normalization of the signals using the quantile normalization algorithm without background subtraction, and differentially regulated genes were defined by calculating the SD differences of a given probe in one-by-one comparisons of samples or groups. Gene expression was considered significantly changed for p values of 0.005 or lower, a fold change of at least ±2 and a greater than 12-fold difference between the bead standard error of treatment and control samples.

cDNA synthesis and quantitative real-time PCR (qRT-PCR) for UPR genes

Three micrograms of total RNA were reverse transcribed with the QuantiTect Reverse Transcription kit (Qiagen). The cDNA was used for quantitative PCR assays performed with the QuantiFast SYBR Green PCR kit (Qiagen) on a DNA Engine Peltier Thermal Cycler Chromo4 (Bio-Rad Laboratories, Germany) and the software Opticon Monitor for measuring gene expression. Beta-actin was used as internal control. The following primers were used: ATF3, 5′-AAG GATTTTCAGCACCTTGC-3′ (forward) and 5′-GA TGGCAGAAGCACTCACTT-3′ (reverse); GADD153, 5′-GCGCATGAAGGAGAAAGAAC-3′ (forward) and 5′-T CTGGGAAAGGTGGGTAGTG-3′ (reverse); XBP-1, 5′-C TGGAACAGCAAGTGGTAGA-3′ (forward) and 5′-CTGG

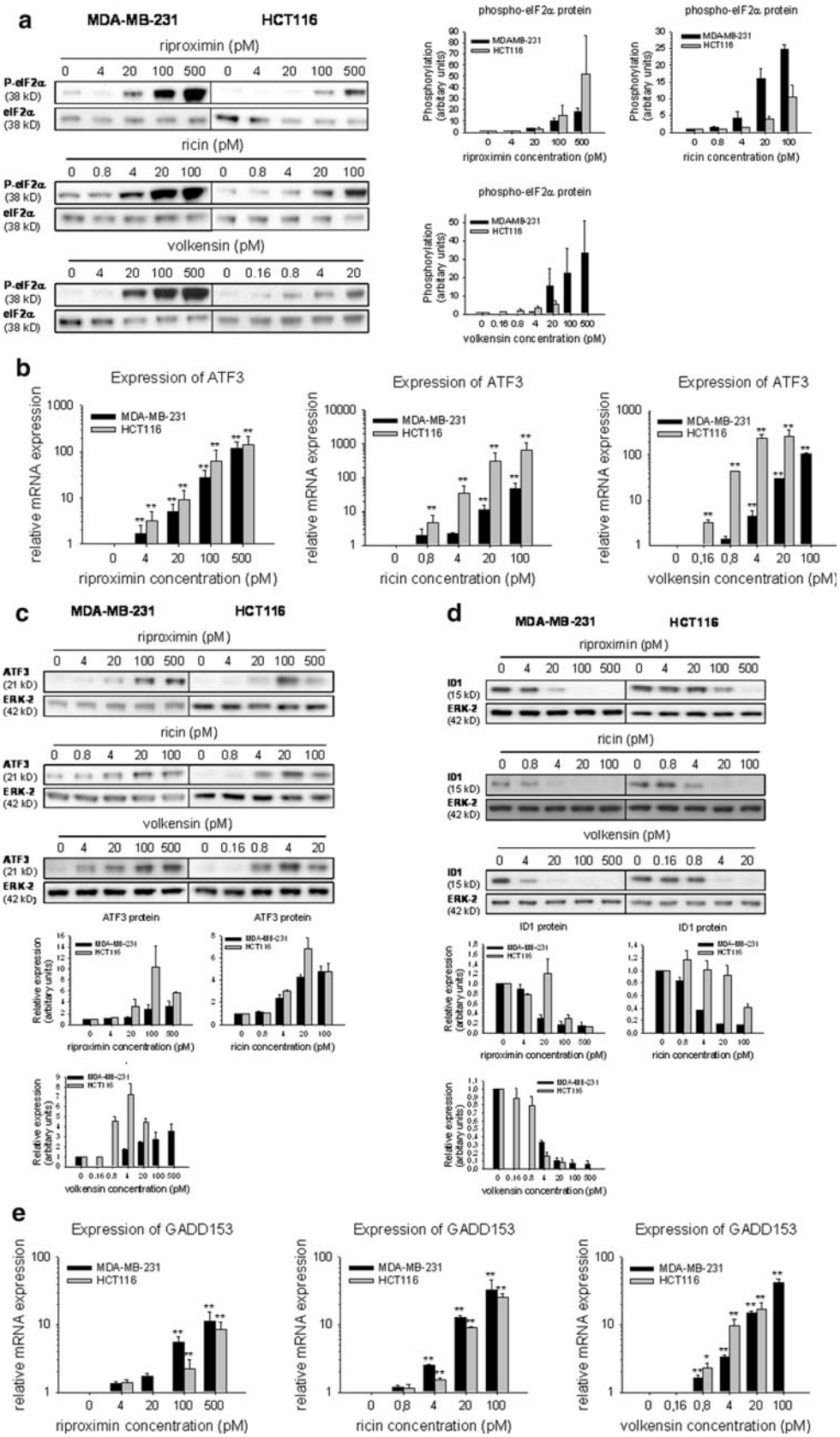

Fig. 3 Activation of the PERK pathway. MDA-MB-231 and HCT116 cells were incubated for 24 h with a range of RIP concentrations as indicated in the respective charts. **a** Protein lysates were directed to immunoblot analysis against phosphorylated eIF2α. Unphosphorylated eIF2α served as loading control. **b**, **e** The relative gene expression of ATF3 and GADD153 at RNA level compared to untreated controls was determined by qRT-PCR. β-actin was used for normalization of the samples. Data are given as mean fold change $\pm$ SE of two to four independent experiments, each performed in triplicate. $^{*}p < 0.05$, $^{**}p < 0.005$ (comparison between control and treatment). **c**, **d** Protein lysates were directed to immunoblot analysis against ATF3 and ID1. ERK-2 served as loading control. All immunoblots were performed two to three times with similar results. One representative blot is shown, respectively. Graphics show mean $\pm$ SD of densitometric analysis of two to three immunoblots for each protein tested

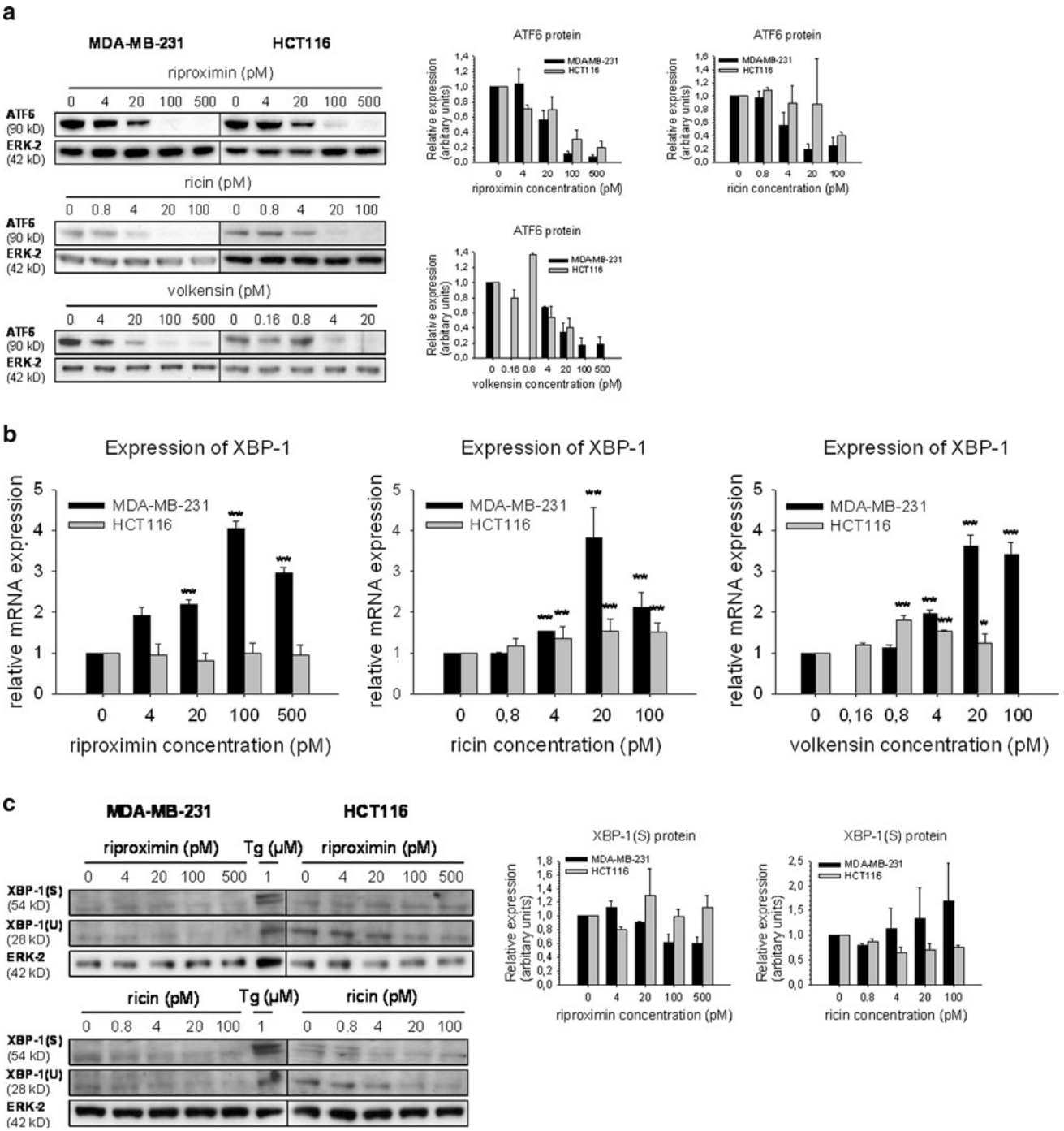

Fig. 4 Activation of the ATF6 pathway, but not of the IRE1 pathway. MDA-MB-231 and HCT116 cells were incubated for 24 h with a range of RIP concentrations as indicated in the respective charts. **a** Protein lysates were directed to immunoblot analysis against ATF6α. ERK-2 served as loading control. **b** The relative gene expression of XBP-1 at RNA level compared to untreated controls was determined by qRT-PCR. β-actin was used for normalization of the samples. Data are given as mean fold change ± SE of two to four independent experiments, each performed in triplicate. $*p < 0.05$, $**p < 0.005$ (comparison between control and treatment). **c** As a positive control, MDA-MB-231 cells were incubated for 4 h with 1 µM thapsigargin (*Tg*). Protein lysates were directed to immunoblot analysis against spliced (*S*) and unspliced (*U*) XBP-1. The antibody detects both isoforms. ERK-2 served as loading control. All immunoblots were performed two to three times with similar results. One representative blot is shown, respectively. Graphics show mean ± SD of densitometric analysis of two to three immunoblots for each protein tested

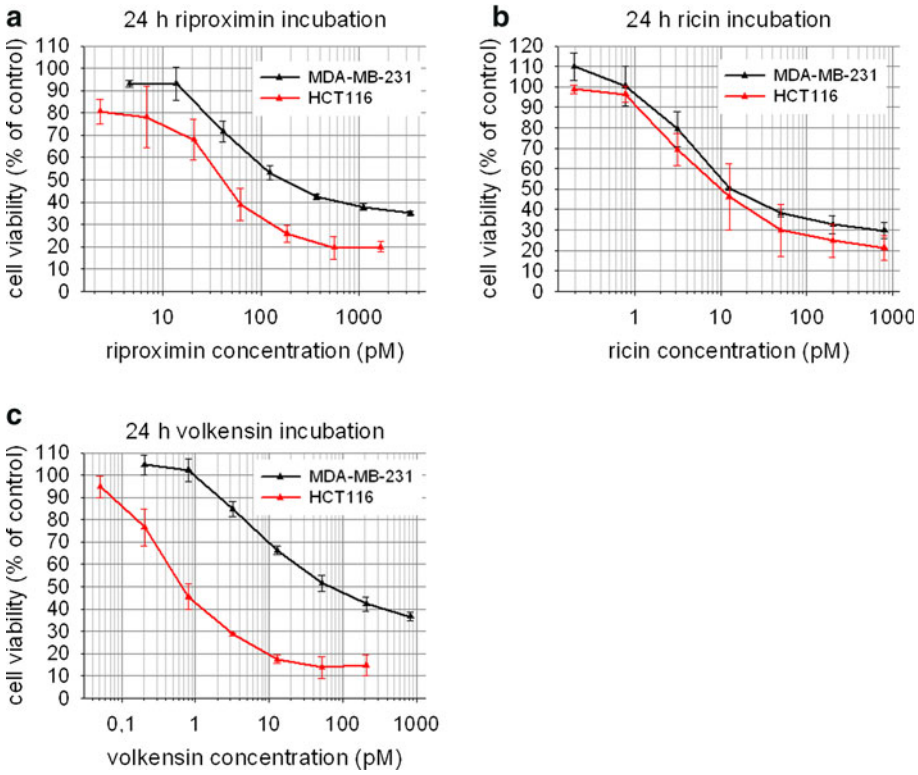

Fig. 5 Change in cell viability upon RIP exposure. MDA-MB-231 and HCT116 cells were incubated for 24 h with a range of riproximin **a**, ricin **b** or volkensin **c** concentrations as indicated in the respective charts. Cell viability was determined by MTT assay. Data are given as mean ± SE

GTCCTTCTGGGTAGAC-3′ (reverse); beta-actin, 5′-AGC CTCGCCTTTGCCGA-3′ (forward) and 5′-CTGGTGCC TGGGGCG-3′ (reverse). The XBP-1 primer pair detects the spliced and the unspliced isoform. The relative gene expression changes—given as fold changes compared to untreated controls, which were set to 1—were calculated with GenEx software (MultiD Analyses AB, Göteborg, Sweden) using the $\Delta\Delta C_t$ method. The data represent mean ± SE of two to four independent experiments, each performed in triplicate.

cDNA synthesis and qRT-PCR for apurinic sites

For detection of apurinic sites in the 28S rRNA, the qRT-PCR method of Melchior and Tolleson [19] was applied with some modifications. Briefly, 200 ng of total RNA was reverse transcribed with the High Capacity cDNA Reverse Transcription Kit (Applied Biosystems). Then 4 µl of a 1:40 dilution of the resulting cDNA was used for qRT-PCRs with the QuantiFast SYBR Green PCR kit (Qiagen) on DNA Engine Peltier Thermal Cycler Chromo4 (Bio-Rad Laboratories). The software Opticon Monitor was used for the measurement of gene expression. The reaction volume was 20 µl per tube. A sequence of the 28S rRNA near the apurinic site served as internal control. The following primers were used: 28S rRNA control, 5′-GATGTCGGCTCTTCCTATCATTGT-3′ (forward); 28S rRNA control, 5′-CCAGCTCACGTTCC CTATTAGTG-3′ (reverse); 28S rRNA depurination, 5′- T GCCATGGTAATCCTGCTCAGTA-3′ (forward); 28S rRNA depurination, 5′-TCTGAACCTGCGGTTCCACA-3′ (reverse). The relative gene expression changes—given as fold changes compared to untreated controls, which were set to 1—were calculated with GenEx software (MultiD Analyses AB) using the $\Delta\Delta C_t$ method. The data represent mean ± SE of two independent experiments, each performed in triplicate.

Immunoblotting

Equal protein amounts (15 or 20 µg per lane) were separated by NuPAGE 4–12% Bis-Tris gel SDS-PAGE with MOPS buffer (Invitrogen) under reducing and denaturing conditions. Proteins were transferred to nitrocellulose membranes by the Xcell SureLock Mini Cell system (Invitrogen). Membranes were blocked for 1 h with 5% BSA or 5% non-fat milk prepared with TBST [50 mM Tris-HCl (pH 7.5); 150 mM NaCl; 0.1% Tween-20]. Incubation with the primary antibody was carried out overnight at 4°C. After three washes for 5 min each with TBST, membranes were incubated with the HRP-coupled secondary antibody for 1 h. After three washes for 5 min each with TBST and one wash with TBS, the membranes were visualized using enhanced chemiluminescence (ECL) reagents (GE Healthcare, Piscataway, NJ). Where necessary, membranes were reprobed. In that case they were

Table 1 Micro-array analysis using Illumina Bead Chips after incubation of MDA-MB-231 cells with riproximin

HUGO gene designation[a]	Fold change after 24 h exposure to:[b,c]		Protein group
	45 pM riproximin	350 pM riproximin	
ATF6	1.9	2.4	ER stress sensors
ERN1 (**IRE1**)	4.2	7.2	
EIF2AK3 (**PERK**)	1.0	1.4	
ATF3	23.8	52.6	Cytosolic effectors
DDIT3 (**GADD153**)	7.0	8.8	
EDEM1	−2.0	−2.3	
GADD45A	12.9	15.7	
GADD45B	6.2	7.2	
IL24	35.4	30.2	
PPP1R15A (**GADD34**)	3.8	3.8	
SERP1 (**RAMP4**)	−1.2	−1.2	
TANK (TRAF2)	1.5	3.6	
XBP1 (**XBP-1**)	1.5	−1.6	
DNAJB11 (**HEDJ**)	−1.2	−1.1	Chaperones and co-chaperones
HSPA1B	−2.5	−2.1	
HSPA5 (**BiP**)	−2.2	−2.3	
HSPA8	−2.9	−12.4	
HSPB1	−2.1	−2.1	
HSPB8	2.8	5.6	

[a] Gene designations in bold were used throughout the text

[b] MDA-MB-231 cells were incubated for 24 h with riproximin concentrations corresponding to IC_{25} and IC_{50} values

[c] Fold change in mRNA expression compared to untreated controls. Changes greater than twofold are significant ($p < 0.005$)

incubated for 20 min at 80°C in stripping buffer [200 mM Glycin (pH 2.5); 0.05% Tween-20], followed by three washes with TBS, each for 10 min. Then the detection started again with the blocking step. All immunoblots were performed two to three times, respectively, for each protein tested. Immunoblots were densitometrically analyzed using Photoshop CS3, and the data are given as mean ± SD after normalization against the respective levels of ERK-2.

DAPI staining of nuclei

A total of 5×10^4 MDA-MB-231 cells were seeded in Lab-Tek four-chamber slides (Nunc, Langenselbold, Germany) and cultured for 24 h. After incubation with 500 pM riproximin, 100 pM ricin or 500 pM volkensin for another 24 h cells were directed to DAPI staining for determination of the amount of fragmented nuclei. All steps were performed at room temperature. The cells were rinsed briefly with PBS and fixed for 15 min with 4% paraformaldehyde/PBS (137 mM NaCl, 2.7 mM KCl, 10.1 mM Na_2HPO_4, 1.8 mM KH_2PO_4, pH 7.4). Three washes for 5 min each with PBS were followed by staining with DAPI (1 µg/ml in H_2O) for 1 min. After another wash with PBS, samples were mounted in Mowiol and allowed to dry over night at 4°C in the dark. Bright field imaging was performed on a Zeiss Cell Observer microscope (Carl Zeiss MicroImaging, Jena, Germany), with a 20× objective.

Statistical analyses

Changes in gene expression measured by qRT-PCR (for quantification of UPR genes and depurination) were given as fold change relative to an untreated control, which was set to 1. The data represent mean ± SE of two to four independent experiments, each performed in triplicate. Where appropriate, the relative fold changes were displayed on a logarithmic scale. The raw data were evaluated with a mixed linear model with fixed effect concentration and random intercept for the nested factor of each measurement within an experimental series using PROC MIXED in SAS software (Version 9.1, SAS Institute, Cary, NC). Dunnett or Dunnett-Hsu pairwise comparisons to control were performed. One asterisk denotes a significance level of $p < 0.05$; two asterisks denote a significance level of $p < 0.005$, both in regard to comparisons between a treatment condition and the respective control.

Results

Type II RIPs depurinate the 28S rRNA

The postulated mode of action of RIPs, an irreversible depurination of a specific adenine in 28S rRNA leading to translational arrest, is normally shown in cell-free systems, but can also be detected in living cells [20]. To verify

depurination for riproximin and ricin in intact HCT116 and MDA-MB-231 cells, a recently developed qRT-PCR method [19] was applied that can be used for intracellular detection of apurinic sites. In both cell lines a concentration-dependent increase of apurinic sites in 28S rRNA was detected upon RIP exposure (Fig. 2). In MDA-MB-231 cells, the relative amount of apurinic rRNA increased by 95- to 163-fold in response to riproximin (500 pM) or ricin (100 pM). Even the lowest concentrations of riproximin (4 pM) and ricin (0.8 pM)—according to IC_0–IC_{20} (Fig. 5a–c)—caused a 3- to 12-fold increase in apurinic rRNA sites compared to untreated controls. HCT116 cells showed a slightly different pattern. The highest levels of apurinic sites (80- to 342-fold increase over control) were measured following incubation with the second highest concentrations, respectively (20 pM ricin or 100 pM riproximin), whereas exposure to the highest RIP concentrations did not further increase the relative amount of apurinic rRNA in this cell line.

Riproximin induces the expression of UPR genes

RNA from MDA-MB-231 cells exposed to different concentrations of riproximin—corresponding to IC_{25} and IC_{50} values—was used for micro-array analysis of 23,000 annotated human genes. It was striking that among the 2,000 significantly modulated genes, those belonging to the UPR were distinctly altered in their expression (Table 1). The expression levels of two of the three UPR sensors were significantly increased: ATF6 was upregulated 2.4-fold and IRE1 7.2-fold in response to 350 pM riproximin, whereas the RNA level of PERK showed no significant change. The expression of ATF3, which is an integral part of the UPR, was strikingly increased: 23.8-fold in response to 45 pM riproximin and 52.6-fold following incubation with 350 pM riproximin. The cytosolic effectors belonging to the group of growth arrest and DNA damage inducible genes (GADD34, 45A, 45B, 153) were 3.8- to 15.7-fold elevated. The expression levels of several chaperones were altered, too, ranging from 2.1- to 12.4-fold compared to controls. It is noteworthy that IL24 was also strikingly induced (30.2- to 35.4-fold), as this cytokine represents a link between the UPR and apoptosis [21].

These results confirmed and extended our initial hints for riproximin inducing an ER stress response and prompted an extension of the studies by two other cytotoxic type II RIPs, ricin and volkensin. The RIP-dependent activation of UPR pathways emerging from the three transducers PERK, IRE1 and ATF6 was examined in more detail. An initial study on the kinetics of protein expression modulation within 2–72 h after riproximin exposure showed that the changes peaked after 24–48 h. Therefore, we chose this window for all subsequent studies.

Type II RIPs induce the PERK branch of the UPR

The UPR sensor PERK phosphorylates and thereby inhibits eIF2α upon activation by ER stress. All tested RIPs—riproximin, ricin and volkensin—clearly enhanced the phosphorylation of eIF2α after 24 h of exposure in both cell lines tested (Fig. 3a). Starting with low toxic concentrations—in the range of 0.8–20 pM—the signal increased clearly up to the highest concentrations (20–500 pM). Even the second lowest concentrations were sufficient to cause a detectable increase in phospho-eIF2α. Within the UPR signaling cascade, this phosphorylation shuts down cap-dependent protein synthesis while specially structured, UPR-associated mRNAs are translated. Hereupon the expression of some transcription factors like ATF3 and GADD153 is elevated at RNA and protein levels. For investigating this process, qRT-PCRs were carried out. Both transcription factors were notably upregulated at the RNA level. ATF3 was significantly elevated in response to riproximin concentrations as low as 4 pM in both cell lines (Fig. 3b). Exposure to 0.8 pM ricin or 20 pM ricin in HCT116 or MDA-MB-231 cells caused a significant increase in the respective mRNA expression levels. HCT116 cells showed a more pronounced upregulation in response to both lectins. The values increased by more than 100-fold after incubation with 500 pM riproximin and at least 47-fold in response to 100 pM ricin. Exposure to volkensin led to similar results in the two cell lines tested (Fig. 3b).

The protein expression data matched the results at the RNA level (Fig. 3c). ATF3 protein was increasingly expressed after exposure to the same RIP concentrations as used for RNA expression analysis. Volkensin caused a similar induction of ATF3 protein as well. In the course of the UPR cascade, ATF3 suppresses the expression of ID1. Figure 3d shows that incubation with 20 or 100 pM riproximin, 4 pM ricin or 4 pM volkensin was sufficient to clearly diminish the amount of ID1 protein in MDA-MB-231 and HCT116 cells. The transcription factor GADD153, another target of ATF4, was upregulated at RNA level after exposure to riproximin, ricin and volkensin in both cell lines as well, but only at higher concentrations than those effective in increasing ATF3 mRNA levels (Fig. 3e). A minimum of 100 pM riproximin, 4 pM ricin or 0.8 pM volkensin was required for a significant change in the GADD153 mRNA expression level. The increase ranged from 2- to 11-fold following exposure to riproximin (100 or 500 pM), 2- to 32-fold in response to ricin (4–100 pM) and 2- to 43-fold after incubation with volkensin (0.8–100 pM), with MDA-MB-231 cells showing

higher expression levels than HCT116 cells. However, for GADD153 protein no changes in expression level were detected (supplemental material, Fig. S1).

Type II RIPs activate the ATF6 pathway of the UPR, but not the IRE1 branch

In response to an ERS signal, ATF6 is transported to the Golgi apparatus and cleaved. Hereupon its N-terminal fragment is released. This fragment is an active transcription factor that translocates into the nucleus and upregulates the expression of certain target genes, like XBP-1. Figure 4a shows that the uncleaved 90-kDa form of ATF6 started to decline after incubation with 20 pM riproximin, and 4 pM of ricin or volkensin, in both cell lines tested. To prove that this effect was not merely due to downregulation or degradation, the expression of the ATF6 target gene XBP-1 was examined. Figure 4b shows that the mRNA levels of XBP-1 were significantly elevated after exposure of MDA-MB-231 cells to concentrations of 20 pM riproximin, 4 pM ricin or 4 pM volkensin and above. The mRNA level rose up to fourfold in response to 100 pM riproximin, 20 pM ricin or 20 pM volkensin. The HCT116 cells upregulated XBP-1 mRNA less prominently, but also significantly upon RIP exposure. Despite increased XBP-1 mRNA levels, none of the three RIPs elicited IRE1-dependent splicing of XBP-1 (Fig. 4c).

The activation of the UPR induces growth arrest and apoptosis

It is established that ER stress leads to cellular growth arrest and that persistent or strong stress can induce apoptosis. The applied RIP concentrations caused a concentration-dependent inhibition in cell viability (Fig. 5a–c). The proliferation inhibiting concentrations ranged by 3–4 orders of magnitude below those of thapsigargin, a positive control for ER stress (data not shown). The colon carcinoma cell line HCT116 was generally more sensitive to exposure to the three RIPs. Low picomolar concentrations caused a growth inhibition of 0–20%, whereas picomolar toxic concentrations resulted in a decrease of 60–80% compared to untreated controls. For detection of apoptosis the cleavage of PARP [poly (ADP-ribose) polymerase]—an early apoptotic event—was examined. Cleaved 89-kDa PARP was detected in both cell lines after incubation with all three RIPs (Fig. 6a), thus indicating induction of apoptosis. The cleaved protein appeared at concentrations of 100 pM riproximin, 4 pM ricin or 4 pM volkensin and above. As another marker of apoptosis, cleavage of caspase-7 was observed in response to 100–500 pM riproximin in both cell lines investigated (supplemental material, Fig. S2). Late apoptosis was also detected in MDA-MB-231 cells by exposure to the respective highest RIP concentration, as evidenced by the number of DAPI-stained, fragmented nuclei (Fig. 6b).

Discussion

The mode of action of RIPs has been postulated already in the 1980s. Endo et al. [22] discovered the *N*-glycosylase activity of the ricin A-chain, which is able to depurinate a certain adenine (A-4324 in rat ribosomes, A-4605 in human ribosomes) in the 28S rRNA of the large ribosomal subunit. Subsequently, it was proposed that the cytotoxic effects of type II RIPs were mediated by the irreversible inhibition of cellular translation, finally leading to cell death [22, 23]. Since then, all RIPs so far have been shown to possess *N*-glycosylase activity as demonstrated in cell-free systems directly or in cellular translational assays indirectly.

Consistent with this paradigm, in the present work it was found that the plant type II RIPs ricin and riproximin depurinate 28S rRNA in cells exposed to concentrations corresponding to the respective IC_5 or higher. The question whether depurination is necessary for RIP-induced cell death and not just a side effect is being controversially discussed [24–28]. Moreover, it is still not clear how depurination leads to cell death or why an inflammatory response is activated upon RIP treatment in vivo. It was shown that the toxicity of the mistletoe lectin 1 (ML1) depends on the glycosylase activity of the A-chain as demonstrated by a reduced potential to cause cell death using an enzymatically inactive form of this RIP [26]. In contrast, an abrin mutant, which was not able to depurinate 28S rRNA, still induced apoptosis [28]. An enzymatically inactive mutant of the bacterial RIP shiga toxin caused the production of cytokines in intestinal epithelium cells and enhanced expression of several pro-apoptotic and UPR-related genes in leukemic monocytes [25, 27]. Moreover, animals treated with RIPs displayed lesions different from those caused by small molecules that specifically inhibit protein synthesis [24]. Therefore, RIPs seem to exert their toxicity not only by their *N*-glycosylase activity, but also by additional mechanisms.

The results of a micro-array using RNA from riproximin-exposed cells indicated that an ER stress response may be involved in the cytotoxicity of this new type II RIP, as genes connected to the UPR—such as ATF3, GADD153 and IL24—were most strikingly, concentration-dependently upregulated. The increased expression of ATF3 and GADD153 was confirmed by qRT-PCR for riproximin. Moreover, ricin and volkensin were shown to induce similar effects. These findings are consistent with the accumulation of cytotoxic RIPs of type II in the

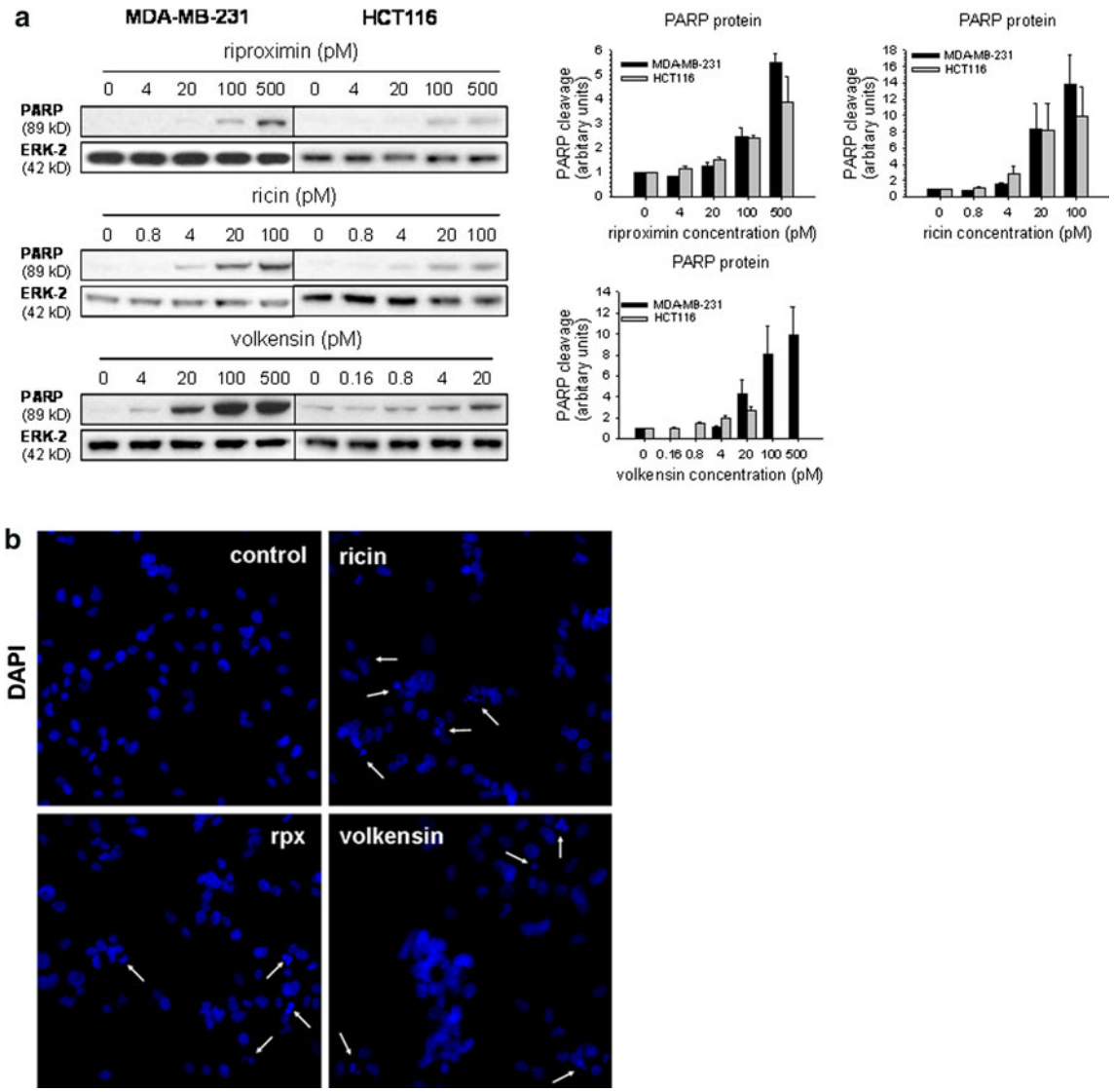

Fig. 6 Induction of apoptosis. MDA-MB-231 and HCT116 cells were incubated for 24 h with a range of RIP concentrations as indicated in the respective charts. **a** Protein lysates were directed to immunoblot analysis against cleaved PARP. ERK-2 served as loading control. Immunoblots were performed two to three times with similar results. One representative blot is shown, respectively. Graphics show mean ± SD of densitometric analysis of two to three immunoblots for each protein tested. **b** Nuclei of MDA-MB-231 cells were stained with DAPI (*blue*), and pictures were taken using a Zeiss CellObserver microscope with a 20× objective. The total number of late apoptotic cells is underestimated as they detach easier from the slide by washing steps than slightly damaged cells

endoplasmic reticulum after passing the *trans*-Golgi network upon receptor binding and cellular entry [29].

We also assessed the three known UPR pathways at the protein level, which are initiated by their sensors PERK, ATF6 and IRE1, as the general translational arrest (caused by depurination) was expected to interfere with the induction of these signaling pathways. The PERK and ATF6 branches of the UPR were concentration-dependently activated by all three RIPs. The third signaling pathway, which involves splicing of XBP-1 by IRE1, was not activated after exposure to RIPs. That coincides with a study in yeast that revealed the inhibition of the XBP-1 homologue Hac1 by ricin A-chain [30]. The assumption that splicing of XBP-1 is inhibited by RIPs is confirmed by the observation that many chaperones that are dependent on spliced XBP-1, like EDEM1, RAMP4 and HEDJ, were not found upregulated at the RNA level (Table 1). Nevertheless, the other functions of IRE1, which are independent of the enzymatic activity of this protein, like activation of JNK that in turn leads to several effects like induction of apoptosis, autophagy and inflammation [31], may play a role in the toxicity of RIPs. In this context, the high expression of IL24 in cells exposed to riproximin was remarkable, as this protein represents a link between UPR

activation and the induction of cell death [21]. As all investigations were carried out in cancer cells, we cannot exclude that normal cells might react differently, i.e., with more or less induction of UPR and related toxicity to RIP exposure.

The data of the present work demonstrate that toxic plant type II RIPs like ricin, riproximin and volkensin induce the UPR. In this study, depurination of the 28S rRNA as well as UPR induction were detected at comparable, low concentrations. However, ribosomal damage did not completely inhibit translation as evidenced by the enhanced protein expression of the UPR gene ATF3. Only at highly toxic concentrations (IC_{75}–IC_{80}), a decrease in the synthesis of ATF3 was observed, whereas ribosomal depurination had reached a plateau. Further work is needed to clarify the relative impact of the UPR vs. ribosome depurination on the cellular translational arrest caused by type II RIPs. However, apoptosis induction at low RIP concentrations, as monitored by the cleavage of the caspase substrate PARP and of caspase-7, does not depend on a general protein synthesis arrest because translation of the UPR-related protein ATF3 still occurred. Therefore, a general inhibition of protein synthesis as postulated for type II RIPs cannot be responsible for induction of apoptosis at low concentrations. Based on these observations we assume that only high RIP concentrations are able to hinder protein synthesis to an extent that unavoidably leads to cell death.

Independent from depurination, UPR-induction alone is, however, sufficient to explain the cellular effects elicited by RIP exposure. UPR causes an arrest of the cap-dependent protein synthesis, whereas specially structured mRNAs like ATF3 are still translated. Apoptosis, autophagy and the production of inflammatory cytokines and chemokines are induced following persistent ER stress via UPR, too [31].

Our findings could be of major importance, because the toxic type II RIPs, particularly ricin, exhibit a potential threat as biological weapons. To deal with toxin misusage, ricin vaccination has been considered [1]. Our findings, however, open a new perspective regarding the treatment of acute type II RIP intoxication. As cells can cope with RIP exposure to a certain extent, substances that inhibit the three UPR pathways might be effective as type II RIP antidotes.

On the other hand, type II RIPs are still of interest as cancer therapeutics. ER stress and the signaling pathways of the UPR also represent new targets for cancer treatment, since many cancer cells activate the UPR in order to cope with stress factors. Two strategies are conceivable in order to exploit the ER stress-related targets: (1) inhibition of the UPR, which prevents the adaptation of cancer cells to stressful settings, or (2) overloading of the cellular UPR machinery to induce apoptosis. Type II RIP exposure should be able to overload the UPR machinery of cancer cells at concentrations that are still well tolerated by normal cells [32]. Apart from the differences in receptor binding, internalization pathways and degradation, the induction of the UPR is probably an important factor contributing to type II RIP specificity against cancer cells [17].

In conclusion, we showed activation of the UPR in cells exposed to ricin, riproximin or volkensin. Although depurination of the 28S rRNA was detected at the same concentrations, our results exclude a general translational arrest resulting from irreversible modification of ribosomes, at least with low and middle growth inhibitory RIP concentrations. As those concentrations also caused induction of apoptosis, we assume that other mechanisms than depurination are responsible for cell death upon exposure to these concentrations of plant type II RIPs. Rather, UPR induction is a mechanism able to explain most of the cellular effects observed following RIP treatment, such as translational arrest, growth inhibition and apoptosis. Further investigations of the RIP-related UPR induction may help to develop more effective and less toxic RIP-based therapeutics for cancer treatment. Additionally, inhibitors of the UPR signaling pathways might be considered and eventually developed as antidotes against RIP intoxication.

Acknowledgments C. Horrix was funded by the DKFZ-MOST program in cancer research. The support by the DKFZ Light Microscopy Facility and the DKFZ Genomics and Proteomics Facility is gratefully acknowledged. Professor Dr. A. Kopp-Schneider, Department of Biostatistics of the DKFZ, is thanked for support with the qRT-PCR statistics.

References

1. Smallshaw JE, Vitetta ES (2010) A lyophilized formulation of RiVax, a recombinant ricin subunit vaccine, retains immunogenicity. Vaccine 28:2428–2435
2. Ng TB, Wong JH, Wang H (2010) Recent progress in research on ribosome inactivating proteins. Curr Protein Pept Sci 11:37–53
3. Stirpe F, Battelli MG (2006) Ribosome-inactivating proteins: progress and problems. Cell Mol Life Sci 63:1850–1866
4. Herrera L, Bostrom B, Gore L, Sandler E, Lew G, Schlegel PG, Aquino V, Ghetie V, Vitetta ES, Schindler J (2009) A phase 1 study of Combotox in pediatric patients with refractory B-lineage acute lymphoblastic leukemia. J Pediatr Hematol Oncol 31:936–941
5. Voss C, Eyol E, Frank M, von der Lieth CW, Berger MR (2006) Identification and characterization of riproximin, a new type II ribosome-inactivating protein with antineoplastic activity from *Ximenia americana*. FASEB J 20:1194–1196
6. Voss C, Eyol E, Berger MR (2006) Identification of potent anticancer activity in *Ximenia americana* aqueous extracts used

by African traditional medicine. Toxicol Appl Pharmacol 211:177–187
7. Voss C. Identifizierung und Charakterisierung des antineoplastischen Wirkstoffs Riproximin, ein neues Ribosomen-inaktivierendes Protein vom Typ 2 aus *Ximenia americana*. Dissertation Medizinische Fakultät, Ruprecht-Karls-Universität Heidelberg. 2005. Ref Type: Thesis/Dissertation
8. Malhotra JD, Kaufman RJ (2007) The endoplasmic reticulum and the unfolded protein response. Semin Cell Dev Biol 18:716–731
9. Verfaillie T, Salazar M, Velasco G, Agostinis P (2010) Linking ER stress to autophagy: potential implications for cancer therapy. Int J Cell Biol 2010:930509
10. Kim I, Xu W, Reed JC (2008) Cell death and endoplasmic reticulum stress: disease relevance and therapeutic opportunities. Nat Rev Drug Discov 7:1013–1030
11. Boyce M, Yuan J (2006) Cellular response to endoplasmic reticulum stress: a matter of life or death. Cell Death Differ 13:363–373
12. Jiang HY, Wek SA, McGrath BC, Lu D, Hai T, Harding HP, Wang X, Ron D, Cavener DR, Wek RC (2004) Activating transcription factor 3 is integral to the eukaryotic initiation factor 2 kinase stress response. Mol Cell Biol 24:1365–1377
13. Ma Y, Brewer JW, Diehl JA, Hendershot LM (2002) Two distinct stress signaling pathways converge upon the CHOP promoter during the mammalian unfolded protein response. J Mol Biol 318:1351–1365
14. Kashiwakura Y, Ochiai K, Watanabe M, Abarzua F, Sakaguchi M, Takaoka M, Tanimoto R, Nasu Y, Huh NH, Kumon H (2008) Down-regulation of inhibition of differentiation-1 via activation of activating transcription factor 3 and Smad regulates REIC/Dickkopf-3-induced apoptosis. Cancer Res 68:8333–8341
15. Yoshida H, Matsui T, Yamamoto A, Okada T, Mori K (2001) XBP1 mRNA is induced by ATF6 and spliced by IRE1 in response to ER stress to produce a highly active transcription factor. Cell 107:881–891
16. Glimcher LH (2010) XBP1: the last two decades. Ann Rheum Dis 69(Suppl 1):i67–i71
17. Battelli MG, Musiani S, Buonamici L, Santi S, Riccio M, Maraldi NM, Girbes T, Stirpe F (2004) Interaction of volkensin with HeLa cells: binding, uptake, intracellular localization, degradation and exocytosis. Cell Mol Life Sci 61:1975–1984
18. Eberwine J, Yeh H, Miyashiro K, Cao Y, Nair S, Finnell R, Zettel M, Coleman P (1992) Analysis of gene expression in single live neurons. Proc Natl Acad Sci USA 89:3010–3014
19. Melchior WB Jr, Tolleson WH (2010) A functional quantitative polymerase chain reaction assay for ricin, Shiga toxin, and related ribosome-inactivating proteins. Anal Biochem 396:204–211
20. Korcheva V, Wong J, Corless C, Iordanov M, Magun B (2005) Administration of ricin induces a severe inflammatory response via nonredundant stimulation of ERK, JNK, and P38 MAPK and provides a mouse model of hemolytic uremic syndrome. Am J Pathol 166:323–339
21. Gupta P, Walter MR, Su ZZ, Lebedeva IV, Emdad L, Randolph A, Valerie K, Sarkar D, Fisher PB (2006) BiP/GRP78 is an intracellular target for MDA-7/IL-24 induction of cancer-specific apoptosis. Cancer Res 66:8182–8191
22. Endo Y, Mitsui K, Motizuki M, Tsurugi K (1987) The mechanism of action of ricin and related toxic lectins on eukaryotic ribosomes. The site and the characteristics of the modification in 28S ribosomal RNA caused by the toxins. J Biol Chem 262:5908–5912
23. Olsnes S, Pihl A (1972) Ricin: a potent inhibitor of protein synthesis. FEBS Lett 20:327–329
24. Battelli MG (2004) Cytotoxicity and toxicity to animals and humans of ribosome-inactivating proteins. Mini Rev Med Chem 4:513–521
25. Colpoys WE, Cochran BH, Carducci TM, Thorpe CM (2005) Shiga toxins activate translational regulation pathways in intestinal epithelial cells. Cell Signal 17:891–899
26. Langer M, Mockel B, Eck J, Zinke H, Lentzen H (1999) Site-specific mutagenesis of mistletoe lectin: the role of RIP activity in apoptosis. Biochem Biophys Res Commun 264:944–948
27. Lee MS, Cherla RP, Leyva-Illades D, Tesh VL (2009) Bcl-2 regulates the onset of shiga toxin 1-induced apoptosis in THP-1 cells. Infect Immun 77:5233–5244
28. Shih SF, Wu YH, Hung CH, Yang HY, Lin JY (2001) Abrin triggers cell death by inactivating a thiol-specific antioxidant protein. J Biol Chem 276:21870–21877
29. Spooner RA, Smith DC, Easton AJ, Roberts LM, Lord JM (2006) Retrograde transport pathways utilised by viruses and protein toxins. Virol J 3:26
30. Parikh BA, Tortora A, Li XP, Tumer NE (2008) Ricin inhibits activation of the unfolded protein response by preventing splicing of the HAC1 mRNA. J Biol Chem 283:6145–6153
31. Schroder M (2008) Endoplasmic reticulum stress responses. Cell Mol Life Sci 65:862–894
32. Healy SJ, Gorman AM, Mousavi-Shafaei P, Gupta S, Samali A (2009) Targeting the endoplasmic reticulum-stress response as an anticancer strategy. Eur J Pharmacol 625:234–246